Electronic Supplementary Material (ESI) for ChemComm.

Freestanding NiS_x Porous Film as Binder-Free Electrode for Mg-Ion Battery

Kun Liang[†,#], *Kyle Marcus*[†, ‡,#], *Limin Guo*[†], *Zhao Li*[‡], *Le Zhou*[‡], *Yilun Li*[‖], *Samuel T. De Oliveira*[¶], *Nina Orlovskaya*[¶], *Yong-Ho Sohn*[‡] & *Yang Yang*[†, ‡,]*

[†]*NanoScience Technology Center, University of Central Florida, Orlando, FL 32826, United States*

[‡]*Department of Materials Science and Engineering, University of Central Florida, Orlando, FL 32826, United States*

[‖] *Department of Chemistry, Rice University, 6100 Main Street, Houston, Texas 77005, United States*

[¶]*Department of Mechanical and Aerospace Engineering, University of Central Florida, Orlando, FL 32826, United States*

*E-mail: Yang.Yang@ucf.edu

Experimental section

Fabrication of NPL. The Ni deposit was obtained through electrochemical deposition. In a typical process, 0.9 M $NiSO_4$, 0.13 M $NiCl_2$, and 0.5 M H_3BO_3 were dissolved in distilled water. The solution was stirred for 60 min at room temperature. A home-made two-electrode system with polished stainless steel foil as cathode and Pt-coated titanium mesh as anode was employed to deposit Ni layer. The cathode current density was set at 20 mA cm^{-2} to perform electrochemical deposition for 7 min. The free-standing Ni layer can be obtained after removing the deposit from the substrate.

After electrodeposition, electrochemical etching was carried out in the same plating electrolyte. The free-standing Ni layer and polished stainless steel foil were used as anode and cathode, respectively. The etching time was 30 s with an anodic current density of 20 mA cm^{-2}. Then, the porous nickel layer was produced after electrochemical etching. Subsequent electrochemically anodic treatment was performed at a current density of 20 mA cm^{-2} for 10 min in the electrolyte of 0.2 M NH_4F with 2 M deionized water in ethylene glycol. The samples were washed with ethanol, deionized water for 3 times, then dried under air gas flow. Finally, NPL was created by electrochemical deposition, etching and anodization.

Fabrication of Nickel sulfides NPL

To convert NiO NPL to NiS_x NPL, the sulfuration was performed in a CVD system with two heating zones. Briefly, S powder and NiO NPL were placed at the upstream and down-stream side of the tube in different heating zones, respectively.

The tube was evacuated to a pressure of 50 mTorr for 10 min and purged with Ar to remove the residual air. Then, the S powder zone and NPL zone were set to 150 and 275 ^{o}C, respectively. The reaction was performed for 30 min with Ar (100 sccm) as carrier gas, followed by natural cooling.

Characterization. A ZEISS ULTRA 55 scanning electron microscope (SEM) and an FEI Tecnai F30 high resolution transmission electron microscope (HRTEM) were used to analyze the morphology and elemental mapping of the samples. X-ray diffraction (XRD) curves were obtained using a PANalytical Empyrean diffractometer (PANalytical B.V.) configured with a Cu Kα radiation. Raman spectra were recorded with a Renishaw Raman RE01 scope (Renishaw, Inc.) using a 532 nm excitation argon laser. X-ray photoelectron spectroscopy (XPS, Physical Electronics) was employed to check chemical composition of the samples.

Electrochemical measurements. Type 2032 coin cells were assembled in a standard two-electrode configuration with NiS_x NPL as the working electrode, Mg foil as the counter electrode, $[AlCl_3][PhMgCl]$/tetrahydrofuran (THF) as electrolyte and Celgard microporous membrane was employed as the separator. The area of the working electrode was 1×1 cm^2. Cyclic voltammetry (CV) was performed in a voltage window of 0.2-2 V at a scan rate of 0.1 mV s^{-1}. Galvanostatic charge/discharge curves were recorded by Landt 2001A test system (Wuhan Land Electronic Co. Ltd., China). The electrochemical impedance spectroscopy (EIS) was collected with frequency range from 10 mHz to 100 kHz using a CHI 760E electrochemical station (CH Instruments, USA).

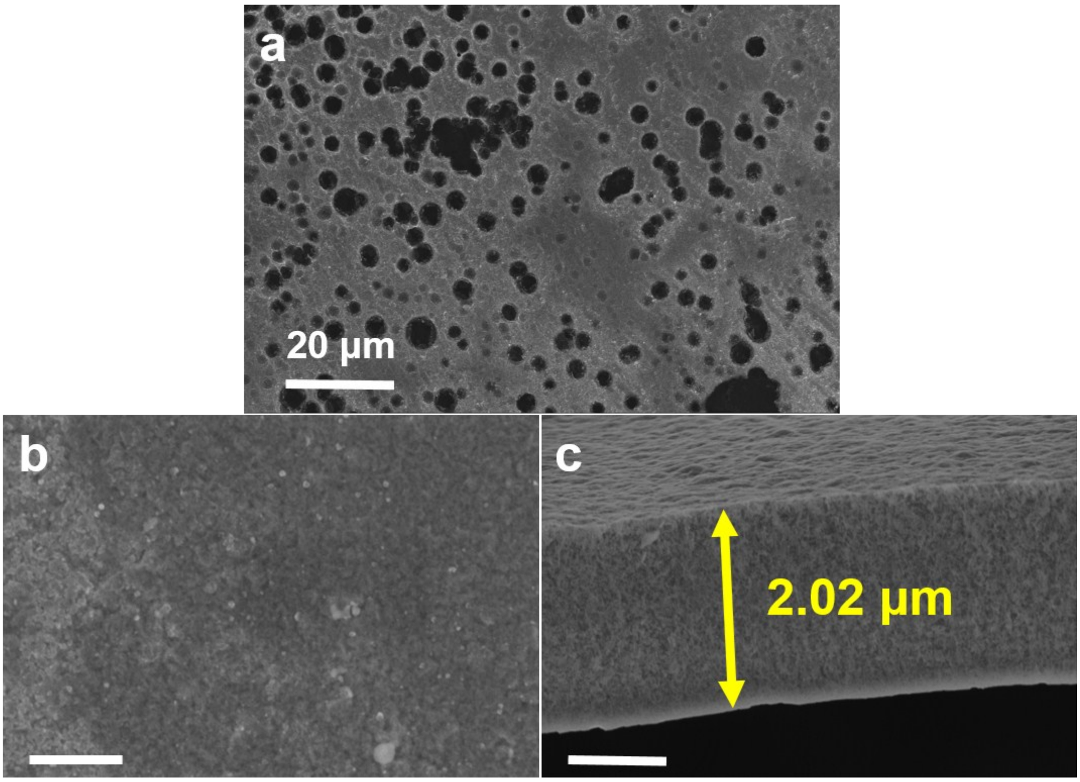

Figure S1. (a) Top-view image of NPL after sulfuration. (b-c) Top-view and cross-sectional images of NPL after sulfuration. The scale bars donate 1 µm.

SEM analysis

Compared with the SEM image in Figure S1b, there are morphology changes that occur after cycling. It should be noted that there is no evidence showing the formation of cracks on the electrode surface. However, aggregated particles with a diameter ranging from 50-200 nm can be observed, caused by the large expansion and shrinkage upon repeated magnesium insertion/extraction. Although the SEM images show that there are morphology changes after cycling, the changes are not substantial, giving the excellent cycling stability.

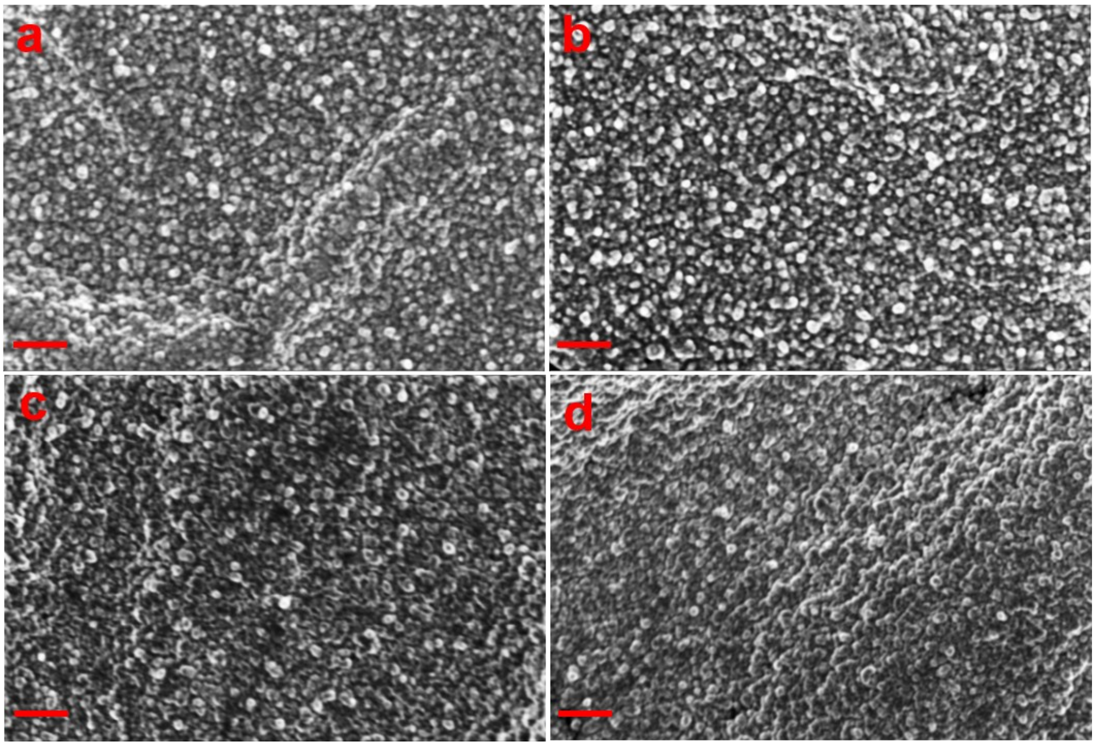

Figure S2. (a-d) SEM images after 100, 500, 1000 and 5000 cycles, respectively. The scale bars donate 1 μm.

XRD and EDS analysis

The peaks of the Ni_3S_2 phase can be found at 21.8°, 37.9°, 49.7°, and 54.9°, while only one peak of the NiS_2 phase can be observed in the XRD pattern. It is noted that the intensities of NiS_2 and Ni_3S_2 were decreased sharply, suggesting that phases reacted with Mg^{2+}. Furthermore, this indicates that both of NiS_2 and Ni_3S_2 are active materials for magnesium-ion battery. An MgS peak can be found located at 30.1° and 34.7°, assigned to (111) and (200) planes, respectively.[1,2] EDS and corresponding elemental mappings after 500 and 5000 cycles were performed. From Figure S4a and S5a, Mg peak can be observed in EDS spectra. Additionally, Mg is uniformly distributed across the surface of the electrode in Figure S4b and S5b, therefore, the final product after charging is MgS.

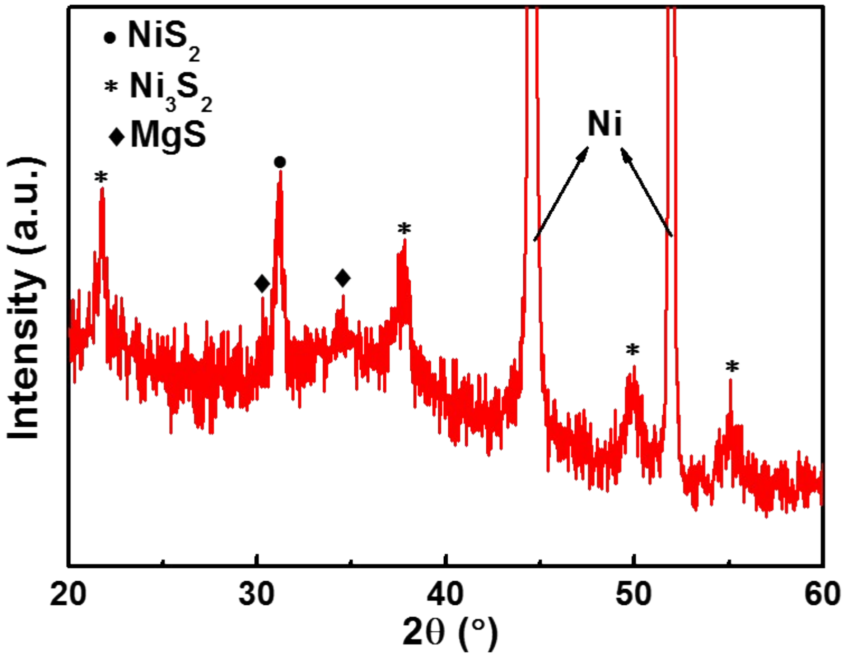

Figure S3. XRD image after 5000 cycles.

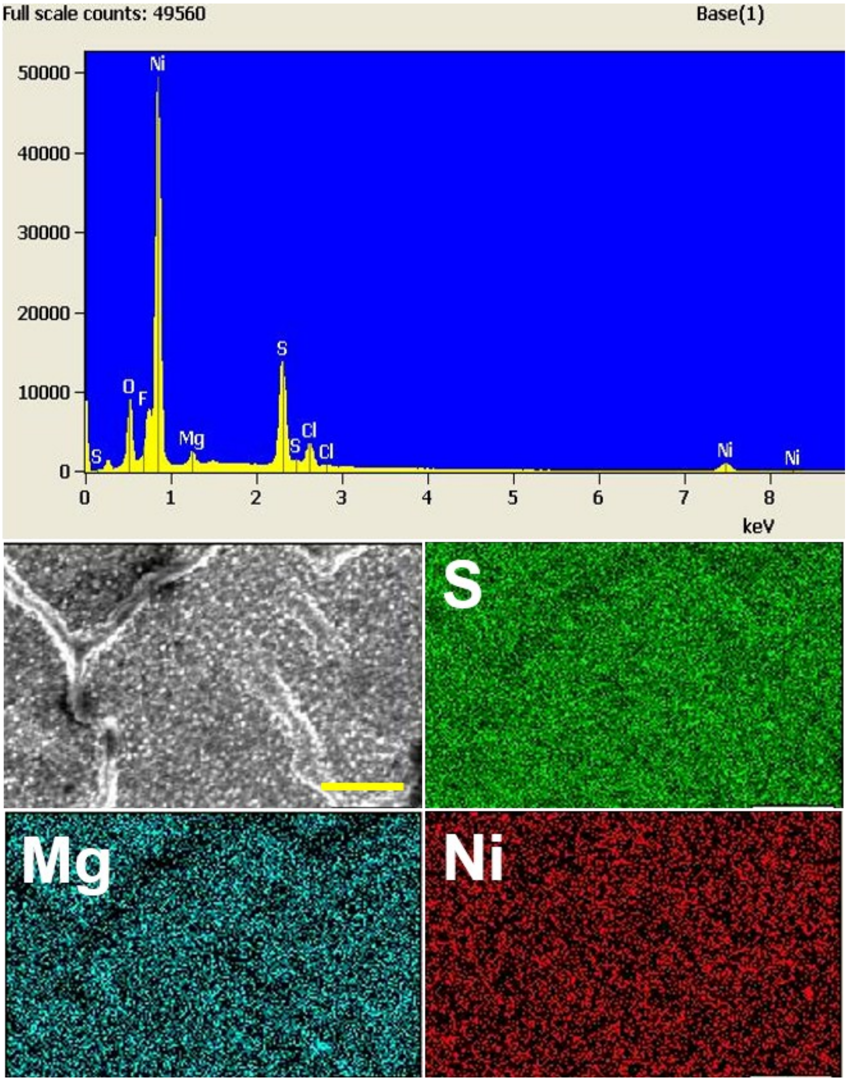

Figure S4. (a-b) EDS spectra and corresponding elemental mapping images after 500 cycles, respectively. The scale bar donates 1 μm.

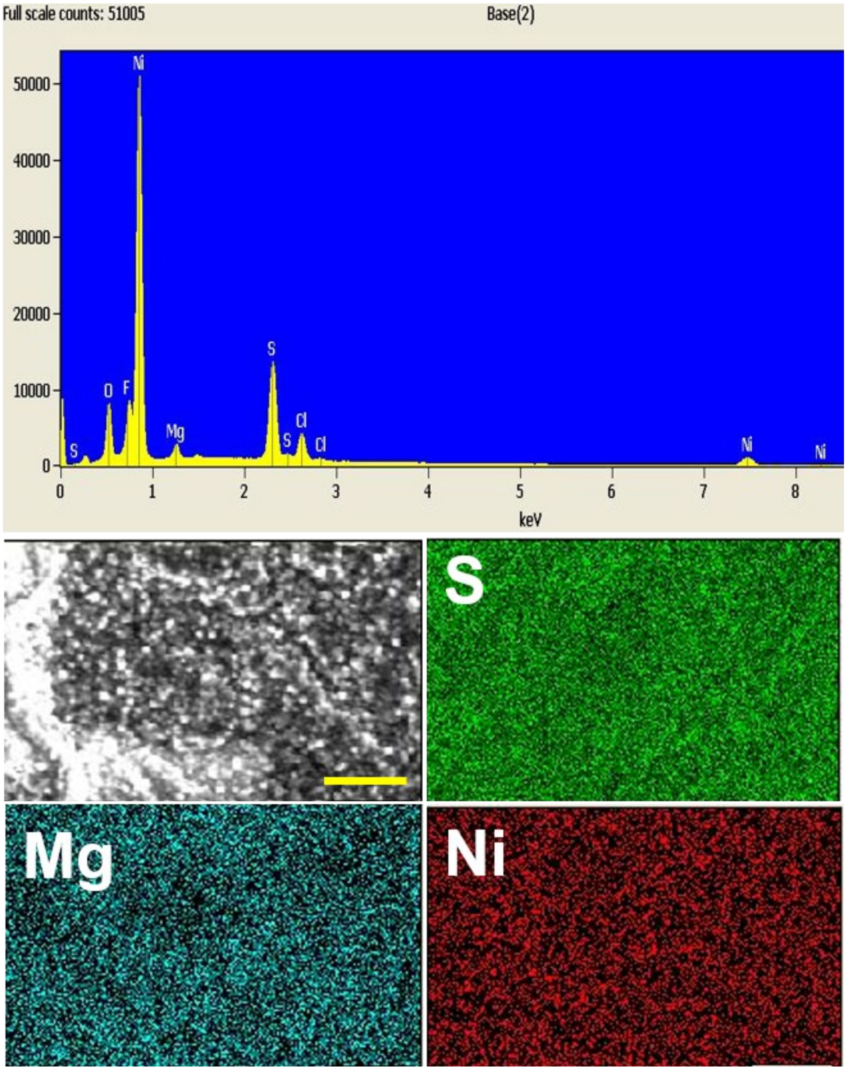

Figure S5. (a-b) EDS spectra and corresponding elemental mapping images after 5000 cycles, respectively. The scale bar donates 1 μm.

EIS analysis

EIS was conducted at room temperature on the cell before and after 5000 cycles to investigate the electrochemical performance of the electrodes. Figure S6 shows the Nyquist plot, presenting the real part and the imaginary part of the impedance. The semicircles in the high-frequency region and the slopes of the straight line in the low-frequency range were different. The bulk solution resistance R_s and the charge-transfer resistance R_{ct} can be obtained from the Nyquist plot, where the high frequency semicircle intercepts the real axis at R_s and $(R_s + R_{ct})$, respectively. Before and after cycling, the bulk solution resistance was increased from 3.8 to 5.6 Ω, while the charge-transfer resistance was increased sharply, which was possibly caused by the loss of active material during the long charge-discharge cycles.

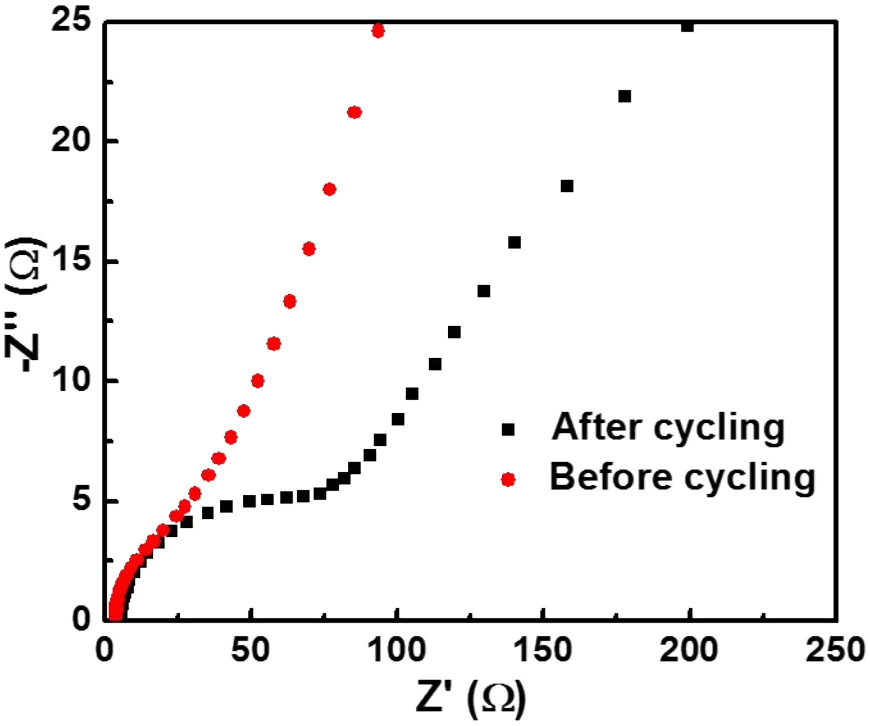

Figure S6. Nyquist plots before and after 5000 cycling.

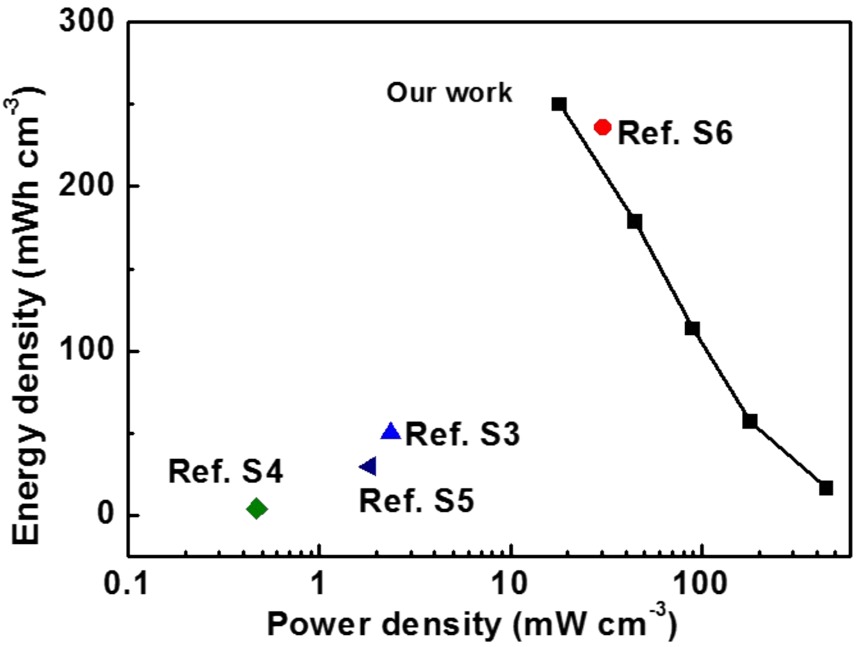

Figure S7. Ragone plot of the NiS_x NPL electrode. The compared MIB systems were reported. [1-4] The volumetric energy density and power density are calculated based on the specific capacity and the volume of the electrode.

Reference

S1. Wang, M., Li, X., Gao, M., Pan, H., Liu, Y., A Novel Synthesis of MgS and its Application as Electrode Material for Lithium-Ion Batteries. *J. Alloy Compd*, **2014**, *603*, 158-166.

S2. Goo, N. H., Hirscher, M., Synthesis of the Nanocrystalline MgS and its Interaction with Hydrogen. *J. Alloy Compd*, **2005**, *404-406*, 503-506.

S3. Zhang, R.; Mizuno, F.; Ling, C., Fullerenes: Non-Transition Metal Clusters as Rechargeable Magnesium Battery Cathodes. *Chem. Commun.* **2014,** *51* (6), 1108-

1111.

S4. Liang, Y.; Feng, R.; Yang, S.; Ma, H.; Liang, J.; Chen, J., Rechargeable Mg Batteries with Graphene-like MoS_2 Cathode and Ultrasmall Mg Nanoparticle Anode. *Adv. Mater.* **2011,** *23* (5), 640-643.

S5. Zhang, R.; Ling, C.; Mizuno, F., A Conceptual Magnesium Battery with Ultrahigh Rate Capability. *Chem. Commun.* **2015,** *51* (8), 1487-1490.

S6. NuLi, Y.; Yang, J.; Wang, J.; Li, Y., Electrochemical Intercalation of Mg^{2+} in Magnesium Manganese Silicate and Its Application as High-Energy Rechargeable Magnesium Battery Cathode. *J. Phys. Chem. C* **2009,** *113* (28), 12594-12597.